Presented at the 54th AIAA Aerospace Sciences Meeting, 4-7 January 2016, San Diego, CA.
Paper AIAA 2016-0599, http://dx.doi.org/10.2514/6.2016-0599

Measurements of Instability in Supersonic Flow with Injection by Time-Resolved Flow Visualization

B. E. Schmidt*and J. E. Shepherd*

Experiments were performed in a Mach 4 Ludwieg tube to examine the transition process in flow over a sharp cone with boundary layer injection. Full-field images with nitrogen, helium, and RC-318 injection reveal that transition occurs earlier with higher injection rates and with lighter injected gas. High-speed imaging at 290 kHz allows the measurement of wavelength and convective velocity by auto- and cross-correlation, respectively, in the cases with nitrogen injection. The wavelength is found to be approximately 8 mm with a convective velocity of 515 m/s, resulting in a frequency range of 60-70 kHz. These properties of the instability waves are roughly constant over all injection rates tested even though the thickness of the injection layer varies by a factor of two.

I. Introduction

Gas injection into boundary layers in supersonic and hypersonic flows has several applications for high-speed flight that could enable new capabilities. The effect of injection on hypersonic boundary layer transition has been studied fairly extensively.[1] Historically, researchers have been interested in injection for cooling applications in hypersonic flows, both in film and transpiration cooling[2–4] and as a surrogate for ablation.[5–8] More recently boundary-layer injection has been studied as a potential means of delaying laminar-turbulent transition in hypervelocity boundary layers due to acoustic absorption[9,10] and in scramjet inlets for a variety of benefits.[11–13]

Injection as a means of cooling on a hypersonic vehicle remains a promising application. Thermal management is a significant issue in hypersonic flight, and the outer surfaces of vehicles are typically covered with a passive thermal protection system such as ceramic tiles. Gas injection has a cooling effect due to the layer of cold gas that flows next to the skin of the vehicle behind the injector.[7] When the gas is injected tangentially to the mean flow direction the effect is called film cooling while when it is injected orthogonally through a porous surface it is called transpiration cooling. Transpiration and film cooling are considered active thermal protection systems, but covering the majority of a vehicle with such a cooling scheme is likely impractical and may not offer significant weight savings compared to traditional passive systems. Localized transpiration cooling, however, has a unique advantage.[14] Passive thermal protection systems do not allow for windows or instruments that would be damaged by the intense heat loads experienced in flight to be placed on the exterior of the vehicle. Localized injection of gas into the boundary layer can provide a limited area of cooling behind the injector where a window or instrument could be located. The cooling is most effective where the layer behind the injector is laminar.

Injection in scramjet inlets is also an active research topic with great potential for enhanced vehicle performance. Researchers have shown that not only does injection of fuel in scramjet inlets by means of porous transpiration have a cooling effect by the same mechanism as outlined above, but it also reduces skin-friction drag, particularly if the fuel is combusted with the air in the free stream.[11] Research also indicates that if the injected stream mixes well with the free stream, then injection of a small fraction of the fuel in the scramjet inlet can enhance combustion efficiency in the combustor and thereby enhance overall engine performance.[13] Finally, because laminar boundary layers are more prone to separation resulting from the compression in scramjet inlets than turbulent boundary layers,[15] the instability created by injection is a desirable effect that can act as a trip that transitions the boundary layer to turbulence before significant compression occurs.

*California Institute of Technology, 1200 E California Blvd, Pasadena, CA 91125

In these applications the stability of the injection layer is of great importance. In cooling applications, the longer the layer can remain laminar the larger the extent of effective cooling. In scramjet inlets, although turbulence mitigates the cooling effect, rapid transition to turbulence is desired for enhanced mixing of fuel and air as well as the added resistance to flow separation. Prior to 2015 no experimental measurements of the instability that leads to transition in this flow had been reported.[1] Schmidt et al[16] report measurements of the wavelength of the instability waves for different injection rates and they find that the measured wavelength agrees well with that of two-dimensional waves predicted by linear stability analysis, but linear stability predicts that oblique waves should contribute most to transition, so the dominant mode in the instability remains unclear. The wavelength was also found to be the same within experimental uncertainty for the two injection mass flow rates studied. The goal of this work is to more carefully measure the properties of the instability waves over a wide range of flow rates in order to draw more definitive conclusions regarding the nature of the instability.

II. Experimental Setup

The experimental facility and model are the same as used in Schmidt et al.[16] The facility is the Mach 4 Ludwieg tube at Caltech, shown in Figure 1. The Ludwieg tube now operates with a fast-acting valve instead of breaking a diaphragm upstream of the nozzle throat as it did prior to 2015. This reduces noise in the free stream, reduces time between experiments, and allows access to a wider parameter space in run conditions. The facility produces Mach 4 flow with nitrogen as the test gas with a freestream velocity of 670 m/s, a steady test time of about 60 ms, and a unit Reynolds number range of 5-25$\times 10^6$ per meter, corresponding to fill pressures between 100 and 600 kPa. The noise level has been reduced to about 0.7% in stagnation pressure, previously it was between 1 and 1.5%. All cases in the current study are performed with a fill pressure of 200 kPa, corresponding to a unit Reynolds number of 9×10^6 per meter and a free stream pressure of 1.2 kPa.

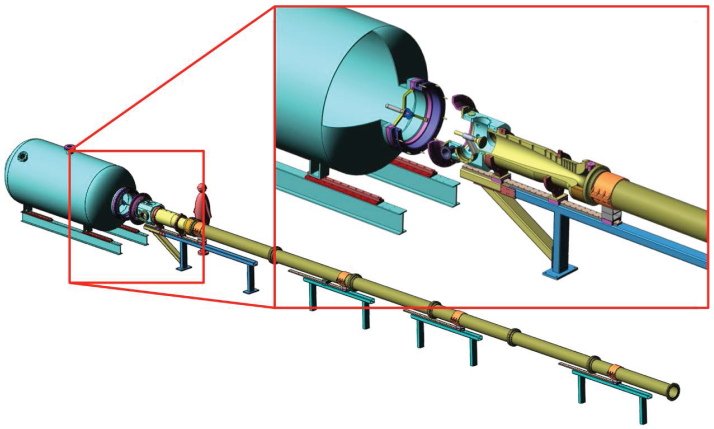

Figure 1: Solid model of the Caltech Ludwieg tube. The overall length of the facility is 23.5 m, the driver tube is 17 m long, and the nozzle exit diameter is 31.5 cm. Test section conditions are $M_\infty = 4$, $T_\infty = 70$ K, $U_\infty = 680$ m/s, and $t_{\text{test}} \approx 60$ ms.

The model used is a sharp-tipped 5-degree half-angle cone with a cylindrical porous injector section. The cylindrical injector geometry is found to minimize the strength of the shock wave formed by injection.[16] Models with cylindrical and frustum-shaped injectors are shown in Figure 2. The shock wave produced by injection with a frustum-shaped injector is observed to significantly promote transition by tripping the boundary layer. Additionally, the total pressure losses associated with this shock and any reflections in an internal flow such as a scramjet inlet are highly undesirable. Therefore only the configuration with the cylindrical injector is tested in the current study, as it allows the natural instability of the injection layer to be observed and because implementation on a vehicle would almost certainly feature some shaping of the injector to mitigate the effects described above. The injector is 40 mm long with a diameter of 23 mm and begins 127 mm from the tip of the cone. The injector is made from sintered stainless steel with a permeability of 3.5×10^{-12} m^2.

Pappas and Okuno observed that gases of different molecular weights cause transition in different locations

for the same injected mass flow rate on a porous cone.[6] Therefore three gases are used in the current study: nitrogen, helium, and RC-318 (octofluorocyclobutane). Nitrogen injection can be simulated easily numerically because the species transport equation decouples from the Navier-Stokes equations. This is not true for helium or RC-318 injection into a nitrogen free stream. Helium has a molecular weight of 4 g/mol, which is 7 times lighter than nitrogen. RC-318 was chosen as a heavy gas because its molecular weight is 200 g/mol, approximately 7 times heavier than nitrogen. RC-318 is a gas at room temperature and is non-flammable, non-corrosive, and non-toxic. It has a ratio of specific heats of 1.054 at room temperature, which means its molecules effectively have 31 internal degrees of freedom. Its sound speed at room temperature is 113 m/s.

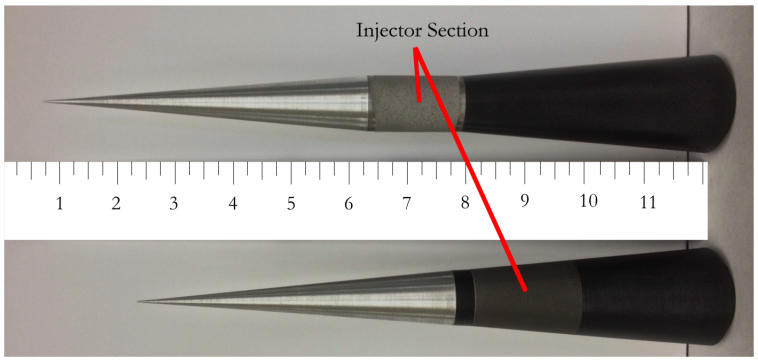

Figure 2: Both models used in the previous study at Caltech.[16] The configuration on top with the cylindrical injector is the one used in the current study. Ruler scale in inches.

The primary diagnostic is a schlieren imaging system using a pulsed laser light source. The details and capabilities of the light source are described in Parziale et al.[17] The current configuration uses a Laser Components 905D3S3J08 laser diode pulsed by a PicoLAS LDP-V 03-100 UF3 laser driver. The diode has a wavelength of 905 nm with a spectral bandwidth of 7 nm. The emitter is a 3 x 3 array of stacked elements with an area of 200 x 250 μm. These properties make the light effectively incoherent, which helps to improve the image quality. The diode has a rated duty factor of 0.1% at an operating current of 30 A, however higher duty factors and pulse rates can be achieved by reducing the operating current. In this study, a current of 3 A was used and the diode was successfully operated at a duty factor of 0.86%. Images are recorded using a Phantom v710 high-speed CMOS camera. A key advantage to the laser light source is that the effective exposure time of the images is determined by the pulse width of the laser, typically tens of nanoseconds, instead of the exposure time of the camera, which is on the order of microseconds. This freezes the motion of fast-moving structures in the flow. Similar systems have been used to measure instability waves in hypersonic boundary layers[18,19] and wake instabilities in high speed flows.[20]

In addition to the imaging system, the model is instrumented with five PCB 132A31 pressure transducers along the length of the cone downstream of the injector. These are sampled at 2 MHz on a National Instruments PCI-6133 data acquisition card. The mass flow rate of the injected gas is measured with an Omega FMA1742A thermal mass flow meter. The thermal flow meter outputs a voltage linearly proportional to the mass flow rate, but the constant of proportionality is dependent on the thermal properties of the gas. The meter was calibrated for each gas with a King Instruments rotameter.

III. Results & Discussion

III.A. Full-field imaging

The first set of experiments performed image the full flow field. Images are recorded at 30,262 frames per second with a pulse width of 40 ns at a resolution of 912 x 240 pixels. The scale for all images is 0.18 pixels per mm. Images from three cases, one with each gas, are shown in Figure 3. The cases were selected such that each has an injection layer thickness δ of 4 mm measured at the rear of the injector as shown in the figure. The injection mass flow rates are normalized by the free stream mass flux to form a parameter F, defined as

$$F = \frac{(\rho u)_{\text{inj}}}{(\rho u)_{\infty}}$$

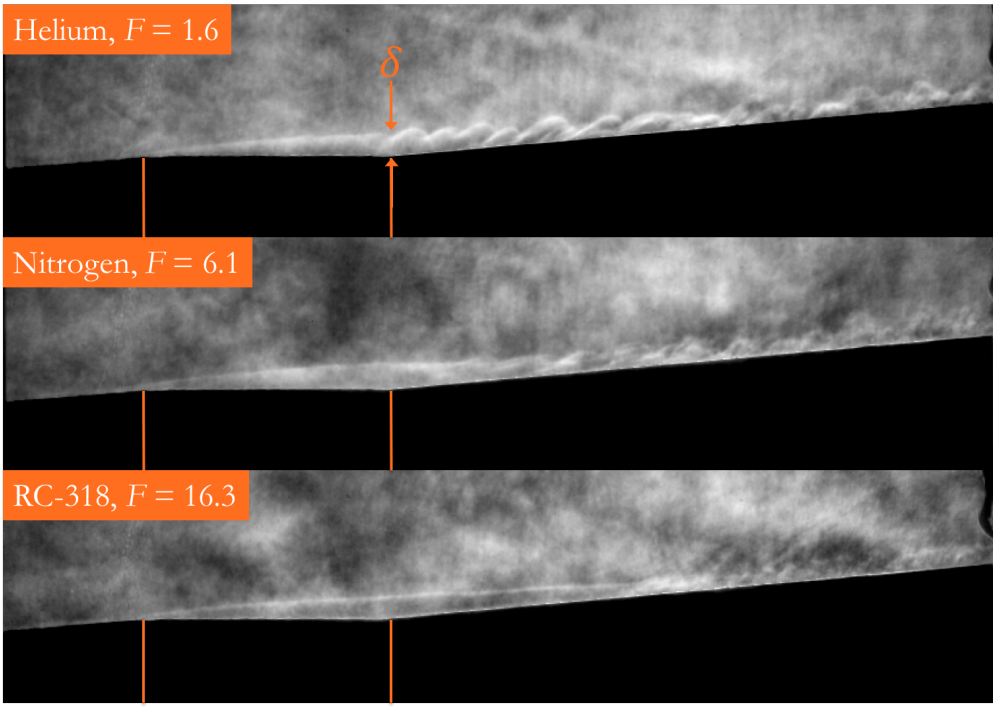

Figure 3: Full-field schlieren images with a 40 ns pulse width for 3 different gases with the same value of δ.

The images in Figure 3 have been minimally post-processed. There is very little speckle in the images, demonstrating the effective incoherence of the light source, although there is some non-uniformity in the illumination. The depth of field of the imaging setup is quite large, on the order of 1-2 meters, due to the small size of the emitter and optical configuration. This causes the system to be sensitive to the shear layers on the outside of the free jet of the wind tunnel flow, which appear as low-amplitude incoherent disturbances in the free stream of the images.

Qualitatively, the properties of the instability for each gas appear to be quite different. Aside from where transition actually occurs, the instability waves differ in appearance. In the first case with nitrogen injection, the waves have rather low amplitude and have a shallow inclination angle to the mean flow. By comparison, in the case with helium injection the waves have much larger amplitude and have a steeper inclination angle, and in the case with RC-318 injection the waves are almost imperceptible and appear only as very low-amplitude, long-wavelength undulations in the laminar interface between the injected gas and the free stream nitrogen before rapidly breaking down to small turbulent eddies. At this time it is unclear whether there is a connection to studies on the effect of density ratio on free shear layers such as Brown & Roshko.[21]

The injection layer thickness δ is plotted versus F for each injected gas in Figure 4. Note that the mass flow rates for the different gases vary a great deal for the same injection layer thickness, which suggests that the mass flux alone is perhaps not the most relevant parameter for determining global flow properties. Mass flux is the parameter used in the literature, however, so its use will be retained here until a more appropriate scaling can be determined.

The location of transition to turbulence can be measured from the set of approximately 1200 images for each case by noting where the interface between the free stream and the injected gas ceases to be smooth and laminar. Transition location is reported here as the dimensional distance in millimeters from the front of the injector because it is not clear how best to compare directly with results from the literature where the entire model or the majority of the model is porous and injecting gas, or if an attempt at a direct comparison is even appropriate. Figure 5 shows the mean transition location with error bars that include the variability in transition location plotted versus F for the three injected gases. The trends observed, that transition is enhanced both by increasing F and by injecting a lighter gas, agree with past observations in the literature.[5]

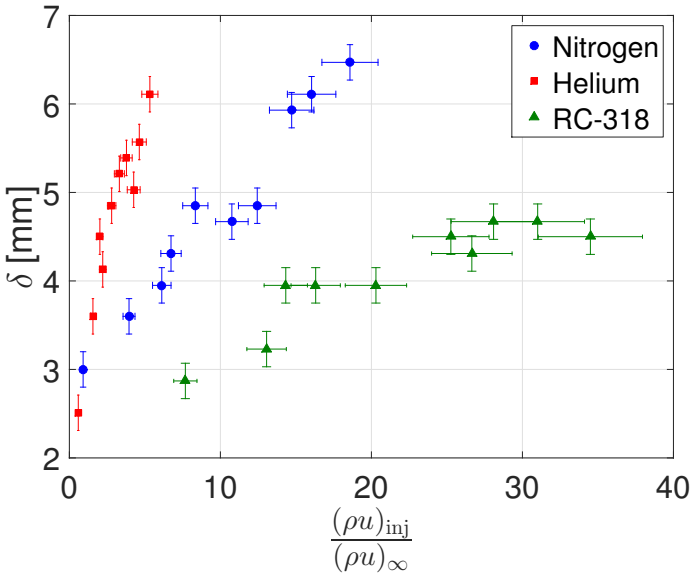

Figure 4: Injection layer thickness δ plotted against non-dimensional mass flux F for each injected gas.

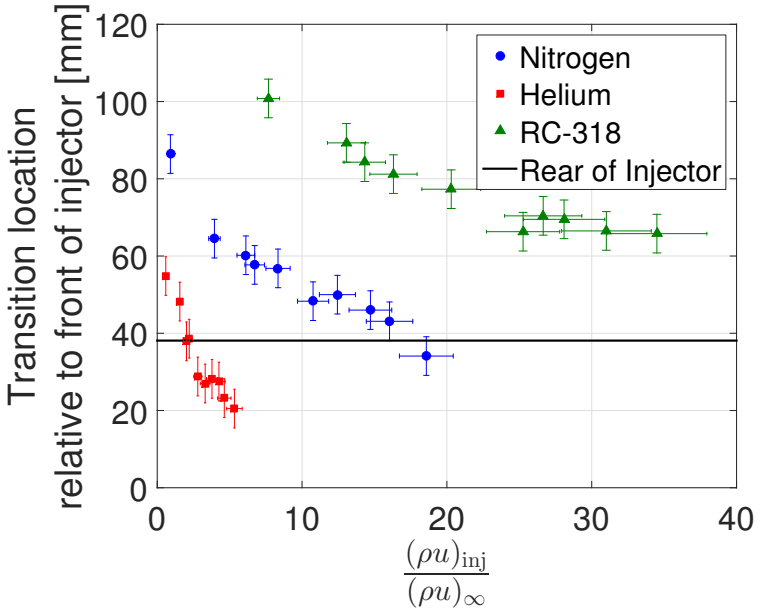

Figure 5: Transition distance from the front of the injector plotted against non-dimensional mass flux F for each injected gas.

III.B. Ultra-high speed imaging

A second set of experiments were performed at a reduced camera resolution of 224 x 64 pixels such that a continuous framing rate of 289361 frames per second can be achieved. The laser pulse width for these experiments is reduced to 25 ns to enhance image freezing and to reduce the duty factor of the laser diode. 10,000 images are acquired for each case, and the convective velocity and wavelength of the instability waves are measured from the set of images. The large number of images acquired allows statistics to be generated from a single case. Only cases with nitrogen injection are included in this paper.

An extensive post-processing routine is used to treat the images so that they can be analyzed. The images are first rotated such that the injection layer is horizontal in the image to simplify determination of the convective velocity. Second, the speckle and other artifacts are removed from each image by calculating the average of the image being processed and 200 images before and after it. A shifting image is calculated

such that when the shifting image is subtracted from the averaged image each pixel has an intensity of 0.5, that is, it is uniformly gray. This shifting image is subtracted from the processing image. After this, the contrast of the image is enhanced uniformly using MATLAB's imadjust function.

At this stage each individual image is of sufficient quality to be analyzed on its own, but the pixel intensity varies significantly from image to image and in different regions of each image which hinders cross-correlation between images and analysis in the time domain. To address this, each column in the image is shifted such that the mean intensity of the column is 0.5. This process results in a set of images that have uniform mean intensity, both across all regions of individual images and one image with respect to another. The final step is to enhance the contrast once more, but the contrast must be increased in a way that does not shift the mean intensity of the image. The intensity map of the image is stretched such that either the darkest pixel is 0 or the brightest is 1, whichever is closest to the current intensity map, and the other pixels are adjusted porportionally such that the mean intensity of the image is maintained at 0.5. Once the image has been thoroughly processed by this routine, the location of the edge of the model is found by using a Canny filter on the averaged image from the second step and the model is set to black in the processed image. Figure 6 shows a sample raw image and the corresponding image after it has been processed.

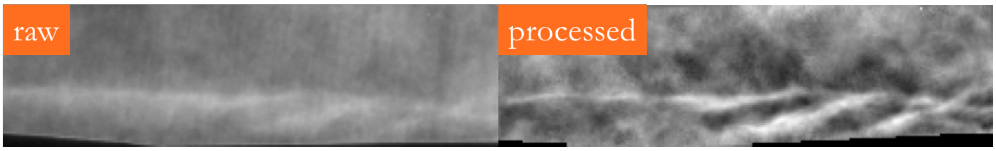

Figure 6: Sample image before and after processing. Instability waves are clearly visible in the processed image.

A common method for determining the wavelength of waves in an image is to sample pixel intensities along a line in the image and perform a spatial Fourier analysis.[19] Such a method is ill-suited for this case for two reasons. First, since the wavelength is a significant fraction of the width of the image, the resolution of the spectra will be poor where the desired peak is expected. Second, coherent structures seldom appear in long chains of more than about four waves at a time in a given image, so there is significant noise present in the spatial spectra, particularly at low wavenumbers.

Instead of using a spectral method, the wavelength is determined by autocorrelation. Figure 7 shows a sample image along with its location relative to the full-field images shown in Figure 3 with the line along which pixel intensities are sampled. Also shown is in Figure 7 is the autocorrelation of the pixel intensities. A peak is observed at about 8 mm, which is the wavelength of the instability waves in the image. The resolution of the autocorrelation in the neighborhood of the wavelength of the instability is approximately 200 μm compared to 2-4 mm for a spectral method.

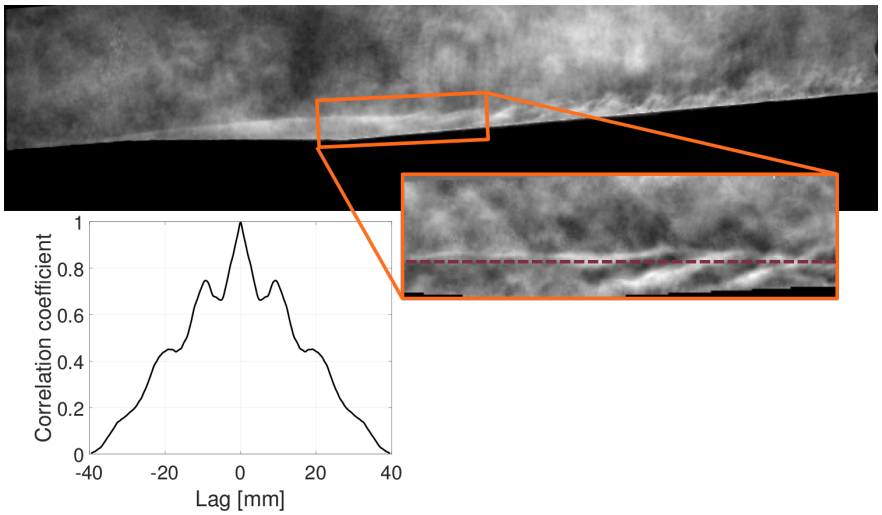

Figure 7: Images are sampled along the dashed line in the figure. The autocorrelation is shown on the left side of the figure. The non-zero peak corresponds to the wavelength of the instability waves.

In order to be considered significant, the peak at non-zero lag in an autocorrelation for a given image must meet two criteria. First, it must be at least 20% higher than the local minimum between the non-zero peak and the peak at zero lag. Second, the value of the correlation coefficient at the non-zero peak must be at least 0.65. These criteria are arbitrary to a degree, but changing the thresholds by small amounts does not change the final result significantly. For a given sample line location in a set of images, between 200 and 400 images out of 10,000 will exhibit non-zero peaks that meet the criteria to be considered significant. An example distribution is shown in Figure 8. Statistics can be computed from the distribution to determine the wavelength for a given case along with an estimate on its variance.

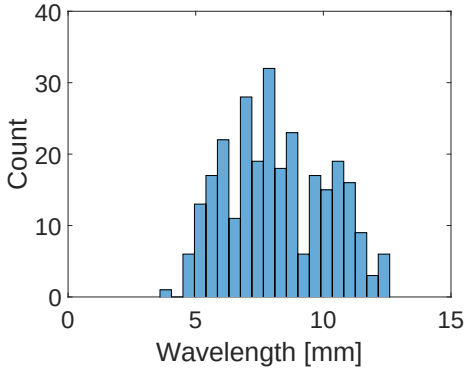

Figure 8: Histogram of wavelengths for the example case shown in Figure 7.

Wavelength data for all nitrogen cases is shown in Figure 9 plotted against F. The data points represent the medians of the distributions for each case with error bars representing standard deviation. The distance from the sample line from the wall on the cone is the one which yields the most images that meet the criteria for significance. Similar to the findings of Schmidt et al,[16] we do not see significant variation of the instability wavelength for the injection rates studied, even though the injection layer thickness δ varies by more than a factor of two.

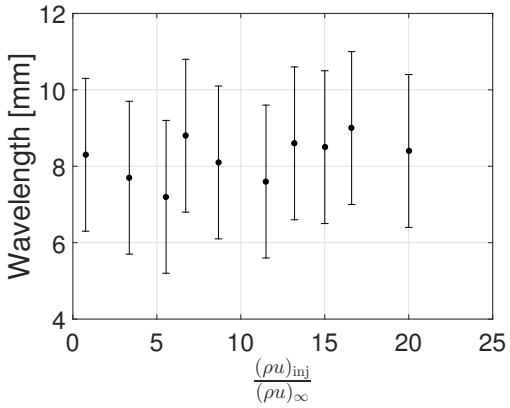

Figure 9: Median instability wavelengths for all nitrogen cases versus F.

Convective velocity of the images can be determined by cross-correlating the pixel intensities along the sample line in each image with those of the previous image. Because images are acquired continuously at a constant frame rate, each image can be correlated with the next. Cross-correlations are considered significant if they have a peak at non-zero lag with a correlation coefficient of at least 0.9. Figure 10 shows a sequence of consecutive images to demonstrate the propagation of a wave packet. The waves move only a few pixels in each image, making cross-correlation quite easy. In a case with 10,000 images, typically 8000-8500 image pairs are correlated enough to be considered significant for acquiring statistics. The cross correlation of two of the images is shown on the right of Figure 10.

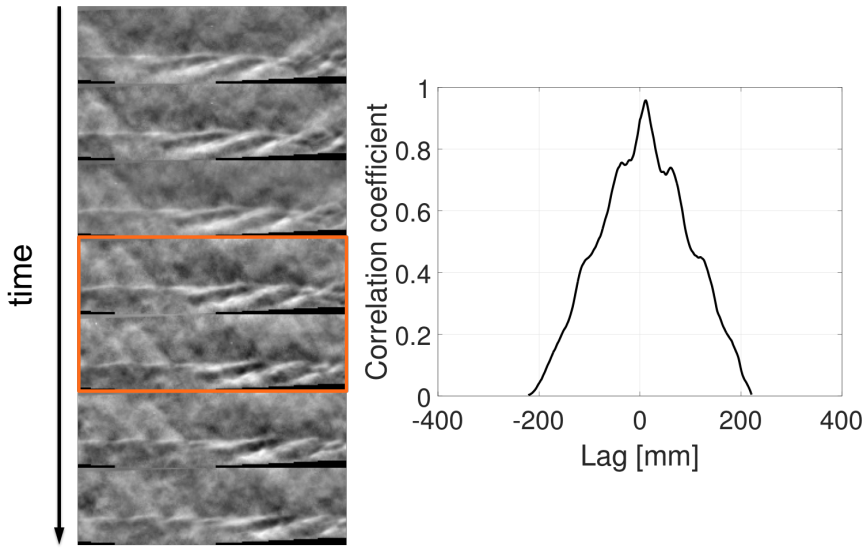

Figure 10: Sequence of consecutive images acquired at approximately 290 kHz. The boxed images are used to produce the cross-correlation curve shown on the right.

A sample distribution of convective velocities is plotted in Figure 11. The plot is a histogram with very narrow bins; the vertical lines in the figure represent individual velocity measurements. To determine the convective velocity a Gaussian is fitted to the histogram. The mean and standard deviation of the Gaussian fit are taken to be the mean and standard deviation of the convective velocity.

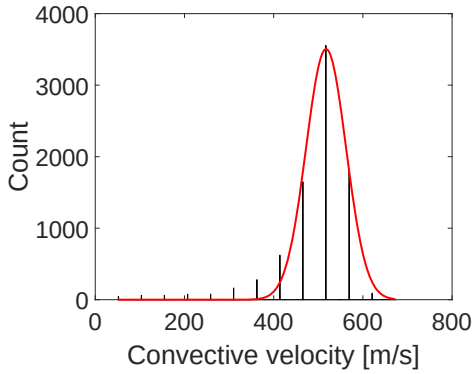

Figure 11: Histogram of convective velocities for the example case.

Convective velocities for all nitrogen cases are plotted versus F in Figure 12. The convective velocity is approximately 520 m/s or 78% of the edge velocity for all injection rates studied with very little variation. For comparison the convective velocity for instability waves in the boundary layer on a straight cone was measured to be 550 m/s or 82% of the edge velocity using the same technique. The convective velocity of structures in a free planar shear layer for the same velocities and densities as the experiment is predicted to be 450 m/s (67% of edge velocity).[22] Clearly the injection layer in the current study is neither a zero-pressure gradient boundary layer nor a planar free shear layer, but the fact that the wavelength and convective velocity show little variation with injection layer thickness suggests that perhaps this instability is more closely related to the Kelvin-Helmholtz instability present in free shear layers than the Mack instabilities[23] that dominate in hypersonic boundary layers.

The frequency of the instability waves is quite difficult to measure directly using the imaging system in the current study both because of noise in the images and because transition is an intermittent process by nature. Signals will inherently contain noise from periods between unstable wave packets. Work is currently underway to develop a scheme that will allow direct frequency measurements with a suitable signal-to-noise

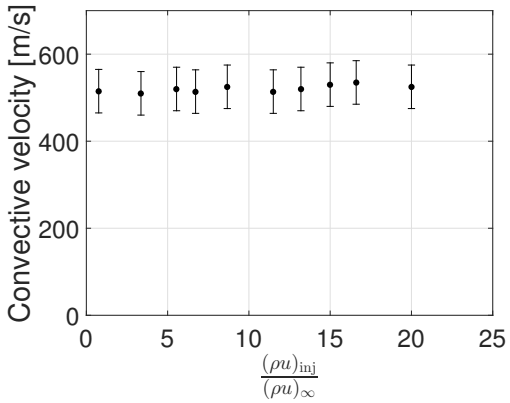

Figure 12: Convective velocity plotted against F for all nitrogen cases.

ratio. The pressure transducers in the model do not show a spectral peak in nitrogen injection cases but they do for a straight cone with no injection. The reason for this is unclear. Either the transducers are all mounted so far behind the transition location in the cases with injection that they cannot measure the waves before breakdown occurs or the instability is localized to the interface between the injected and free stream gases so that pressure fluctuations from the waves do not propagate to the model surface.

The frequency can be calculated in the present study from the wavelength and convective velocity, however, and frequencies are plotted in Figure 13. Similar to the convective velocity and wavelength, the frequency has approximately a constant value for the injection rates studied. Computed frequencies of 60-70 kHz compare reasonably well with the predicted unstable frequencies calculated using linear stability analysis in Schmidt et al.[16]

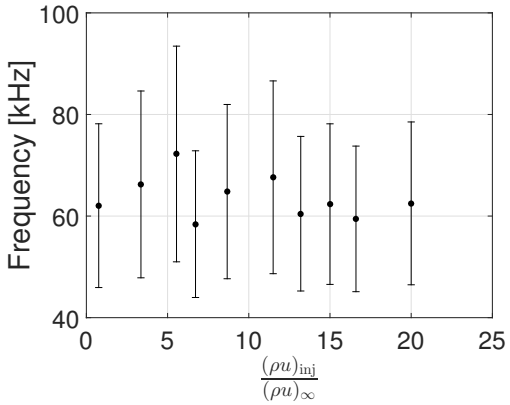

Figure 13: Instability frequencies plotted against F for all nitrogen cases.

IV. Conclusions and Future Work

Injection into supersonic boundary layers is a promising technology for future hypersonic vehicles, but little experimental data exist on the nature of the instability in these flows that leads to transition to turbulence. The current study uses high-speed imaging to measure the frequency of the instability waves in a flow with injection for the first time, and both the frequency and wavelength of the instability do not appear to vary significantly with the distance between the wall and the interface of the injected and free stream gases. The results presented here are preliminary, but suggest that the presence of the wall plays a limited role in determining the properties of the instability waves in the injection layer. The type of gas injected, on the other hand, appears to be more significant. This conclusion suggests that comparisons with studies of supersonic free shear layers may be warranted in the future.

Clearly more work is needed on this subject to fully understand the nature of the instability observed in supersonic flows with injection. As mentioned in Section III.B, work is currently underway to make direct

measurements of the frequency from the imaging data. Techniques for two-dimensional image correlation and object recognition will also be attempted to more rigorously measure the wavelength and convective velocity of the instability waves. The images of cases with helium and RC-318 injection will also be analyzed at least to the extent that the nitrogen cases are analyzed in the present study. Finally, a parameter besides F will be sought to collapse the data in Figures 3 and 4 for cases with different injected gases.

Acknowledgments

Thanks to Bahram Valiferdowsi, Ali Kiani, and Joe Haggerty for assistance with the models used in the present study. Additional thanks are due to Neal Bitter for insights into the transition process in supersonic flows. Bryan Schmidt acknowledges the support of Foster and Coco Stanback STEM Fellowship for his graduate studies.

References

[1]S. P. Schneider. Hypersonic boundary-layer transition with ablation and blowing. *Journal of Spacecraft and Rockets*, 47(2), March-April 2010.

[2]A. M. Cary and J. N. Hefner. An investigation of film-cooling effectiveness and skin friction in hypersonic turbulent flow. In *AIAA 4th Fluid and Plasma Dynamics Conference*. AIAA, June 1971.

[3]B. Aupoix, A. Mignosi, S. Viala, F. Bouvier, and R. Gaillard. Experimental and numerical study of supersonic film cooling. *AIAA Journal*, 36(6), June 1998.

[4]N. Sahoo, V. Kulkarni, S. Saravanan, G. Jagadeesh, and K. P. J. Reddy. Film cooling effectiveness on a large angle blunt cone flying at hypersonic speed. *Physics of Fluids*, 17(036102), 2005.

[5]C. C. Pappas and A. Okuno. Measurements of skin friction of the compressible turbulent boundary layer on a cone with foreign gas injection. *Journal of the Aero/Space Sciences*, 27:321–333, May 1960.

[6]C. C. Pappas and A. Okuno. Heat-transfer measurement for binary gas laminar boundary layers with high rates of injection. Technical Report NASA TN-D-2473, NASA, 1964.

[7]J. G. Marvin and C. M. Akin. Combined effects of mass addition and nose bluntness on boundary-layer transition. *AIAA Journal*, 8(5):857–863, May 1970.

[8]Fei Li, Meelan Choudhari, Chau-Lyan Chang, and Jeffery White. Effects of injection on the instability of boundary layers over hypersonic configurations. *Physics of Fluids*, 25, 2013.

[9]R. M. Wagnild, G. V. Candler, I. A. Leyva, J. S. Jewell, and H. G. Hornung. Carbon dioxide injection for hypervelocity boundary layer stability. In *48th Aerospace Sciences Meeting*, number AIAA 2009-1287, Orlando, FL, 2009. AIAA.

[10]J. S. Jewell, I. A. Leyva, N. J. Parziale, and J. E. Shepherd. Effect of gas injection on transition in hypervelocity boundary layers. In *28th International Symposium on Shock Waves*, pages 735–740. Springer Berlin Heidelberg, 2012.

[11]J. E. Barth, V. Wheatley, and M. K. Smart. Hypersonic turbulent boundary-layer fuel injection and combustion: Skin-friction reduction mechanisms. *AIAA Journal*, 51(9):2147–2157, September 2013.

[12]A. S. Pudsey, R. R. Boyce, and V. Wheatley. Hypersonic viscous drag reduction via multiporthole injector arrays. *Journal of Propulsion and Power*, 29(5):1087–1096, 2013.

[13]D. M. Peterson, R. R. Boyce, and V. Wheatley. Simulations of mixing in an inlet-fueled axisymmetric scramjet. *AIAA Journal*, 51(12):2823–2832, 2013.

[14]I. Egorov, E. Vasilevskii, A. Novikov, and I. Ezhov. Tangential blowing to a supersonic flow on a blunted nose. In *53rd AIAA Aerospace Sciences Meeting*, number AIAA-2015-0212. AIAA, 2015.

[15]D. A. Ogorodnikov, V. T. Grin, and H. N. Zakharov. Controlling the boundary layer in hypersonic air intakes. In *1st International Symposium on Air-Breathing Engines*, number FTD-HT-23-1349-72, June 1972.

[16]B. E. Schmidt, N. P. Bitter, H. G. Hornung, and J. E. Shepherd. Injection into supersonic boundary layers. *AIAA Journal*, 2015. doi: 10.2514/1.J054123.

[17]N. J. Parziale, J. S. Damazo, B. E. Schmidt, P. S. Wang, H. G. Hornung, and J. E. Shepherd. Pulsed laser diode for use as a light source for short-exposure, high-frame-rate flow visualization. In *AIAA SciTech 2015*, number AIAA-2015-0530. AIAA, 2015.

[18]S. J. Laurence, A. Wagner, K. Hanneman, V. Wartemann, H. Ludeke, H. Tanno, and K. Ito. Time-resolved visualization of instability waves in a hypersonic boundary layer. *AIAA Journal*, 50(6):243–246, 2012.

[19]S.J. Laurence, A. Wagner, and K. Hannemann. Schlieren-based techniques for investigating instability development and transition in a hypersonic boundary layer. *Experiments in Fluids*, 55(8), 2014.

[20]B. E. Schmidt and J. E. Shepherd. Oscillations in cylinder wakes at mach 4. *Journal of Fluid Mechanics*, 785, 2015.

[21]G. L. Brown and A. Roshko. On density effects and large structure in turbulent mixing layers. *Journal of Fluid Mechanics*, 64:775–816, 1974.

[22]Dimitri Papamoschou. Structure of the compressible turbulent shear layer. *AIAA Journal*, 29(5):680–681, 1991.

[23]L. M. Mack. Boundary-layer linear stability theory. Technical Report AD-P004 046, Jet Propulsion Laboratory and California Institute of Technology, Pasadena, CA (USA), 1984.